Nuclear Engineering and Design 322 (2017) 165–176

Contents lists available at ScienceDirect

Nuclear Engineering and Design

journal homepage: www.elsevier.com/locate/nucengdes

CFD-simulation of boiling in a heated pipe including flow pattern transitions using the GENTOP concept

T. Höhne [a,*], E. Krepper [a], G. Montoya [b], D. Lucas [a]

[a] Helmholtz-Zentrum Dresden-Rossendorf (HZDR) – Institute of Fluid Dynamics, P.O. Box 510119, D-01314 Dresden, Germany
[b] Department of Nuclear Science and Engineering, Massachusetts Institute of Technology, 77 Massachusetts Ave, Cambridge, MA 02139, USA

HIGHLIGHTS

- Boiling flow inside a wall heated vertical pipe is simulated by a multi-field CFD approach.
- The paper presents the extension of the GENTOP model for phase transfer.
- The simulation of flow regimes transitions during boiling in a pipe is now feasible.

ARTICLE INFO

Article history:
Received 20 March 2017
Received in revised form 12 June 2017
Accepted 28 June 2017
Available online 8 July 2017

Keywords:
GENTOP
AIAD
Two-phase flow
CFD
Boiling
Multiscale

ABSTRACT

Boiling flow inside a wall heated vertical pipe is simulated by a multi-field CFD approach. Sub-cooled water enters the pipe from the lower end and heats up first in the near wall region leading to the generation of small bubbles. Further along the pipe larger and larger bubbles are generated by coalescence and evaporation. This leads to transitions of the two-phase flow patterns from bubbly to churn-turbulent and annular flow. The CFD simulation bases on the recently developed GEneralized TwO Phase flow (GENTOP) concept. It is a multi-field model using the Euler-Euler approach. It allows the consideration of different local flow morphologies including transitions between them. Small steam bubbles are handled as dispersed phases while the interface of large gas structures is statistically resolved. The paper presents the extension of the GENTOP model for phase transfer and discusses the sub-models used. Finally the above mentioned boiling pipe is considered as demonstration case.

1. Introduction

Two-phase flows can be found in various industrial applications: nuclear power plants, processing industries, heat transfer systems, transport systems, and of course also in nature in general (ocean waves, river flooding). Much progress has been achieved in establishing models to describe various multiphase flow phenomena using Computational Fluid Dynamics (CFD).

The Eulerian two-fluid model is most suited for small-scale dispersed flows like bubbly or droplet flows. Here the length scale of interfacial structures is usually smaller than or in the order of the used grid size, therefore an averaged treatment is used and for each phase a corresponding set of equations is solved. The inhomogeneous Multiple Size Group (iMUSIG) model extends the two-fluid model to a multi-field two-fluid approach. It has been successfully applied to very complex dispersed flows consisting of bubbles with different sizes and associated velocity fields (Frank et al., 2008; Krepper et al., 2008). Furthermore, much progress has been made to improve and generalize coalescence- and breakup closures within the Eulerian framework by Liao et al. (2015).

The one fluid approach with interface tracking is used for flow situations with large-scale interfaces like film -, annular – or horizontal stratified flows. The grid has to be fine enough for a localization of the gas-liquid interface allowing a detailed resolution of the surface phenomena. Established methods are straightforward interface tracking methods like surface-attached moving meshes or interface capturing methods like the Volume of Fluid (VOF)- or the Level-Set-method that are developed for the volume fraction advection step. Concerning these basic computational methods still gap remains in the scales for intermediate ranges of interfacial structures pointed out by Tomiyama et al. (2006).

However, many flows in nature and industry show both separated and dispersed flow structures simultaneously. In many applications interfacial structures cover a wide range of scales

* Corresponding author.
E-mail address: t.hoehne@hzdr.de (T. Höhne).

http://dx.doi.org/10.1016/j.nucengdes.2017.06.047
0029-5493/

Nomenclature

a	surface area (m^2)
α	void fraction
a_D, a_B	blending coefficients for droplets and bubbles
A	interfacial area density (1/m)
C_D	drag coefficient
d	diameter (m)
f_j	blending function
F_D	drag force (N)
g	gravitational acceleration (m/s^2)
h	heat transfer coefficient (W/m^2 K)
H	specific enthalpy (J/kg)
L	length scale at the interface (m)
$\dot{m}$	mass flux due to phase transition (kg/s)
n	unit vector to the interface directed from the main to the secondary fluid
p	pressure (Pa)
q	heat flux (W/m^2)
Q	rate of heat transfer (W)
t	time (s)
U	velocity (m/s)
Γ	mass generation
Φ	interfacial dissipation
ρ	density (kg/m^3)
λ	thermal conductivity (W/m K)
τ	shear stress (Pa)

Subscripts

B	bubble
D	drag
Surf	free surface
G	gas
GasC	continuous gaseous phase
GasD	disperse gaseous phase
i	interface
k	phase gas or liquid
L	liquid
Turb	turbulent
W	wall

and frequently transitions between such different morphologies occur. The smallest scales are the order of the smallest bubbles entrained and the largest scales are governed by continuous gas structures formed at the surface. The complexity of the phenomena demands a multi-field simulation. The larger gas structures should be determined by an interface tracking method to resolve the interfaces, but the small gas structures of different sizes require a multi-fluid model for bubbly flows. Neither of the two basic models is enough for the simulation of such a flow phenomenon.

A way to deal with different scales of interfacial structures is to use the Eulerian multi-fluid model equations within the whole computational domain and the implementation of an additional interface sharpening algorithm. It is important to keep in mind that as a result of the averaging procedure in an Eulerian framework the captured interface is filtered and sub-grid information about it has disappeared (Bestion, 2010). The NEPTUNE-code works with a Large Interface Model (LIM) for stratified flows. This model locates the interface without any reconstruction in order to apply closure laws. For this a refined gradient method is used which allows to detect stratified grid cells. The LIM-model has been validated on several configurations (Coste et al., 2010) and has also been compared with other CFD-models within a benchmark (Bartosiewicz et al., 2010).

An alternative type of interface capturing method within the two-fluid model is implemented in the CFX-code using a compressive advection discretization scheme which is applied to the volume fraction equation (Zwart et al., 2007). This so-called Free Surface model has been used successfully for the modeling of horizontally stratified pipe flows (Vallée et al., 2008). Nevertheless, it is not appropriate to represent mixed flows so far as there is the need to identify the morphology of the fluid phases. An Algebraic Interfacial Area Density (AIAD)-model was introduced by Höhne and Vallée (2010). This model simulates the momentum exchange dependent on the morphological form of the stratified flow pattern and distinguishes between bubbles, droplets and the interface using the liquid volume fraction values. It was implemented into the CFX-code and validated against experimental data of counter-current flows in a hot leg model of a pressurized water reactor (Höhne et al., 2011), in horizontal channels (Höhne and Mehlhoop, 2014) and at the Wenka test facility (Porombka and Höhne, 2015). The AIAD-model represents a new alternative way to capture the gas-liquid interface within the two-fluid model.

Olsson and Kreiss (2005) introduced a level set method in which the advection of the level-set function is followed by an artificial compression step to ensure that the thickness of the interface layer is preserved, inducing a volume conservation. Štrubelj et al. (2009) improved the two-fluid model with a conservative level-set method proposed by Olsson and Kreiss (2005). Additionally the model included a surface tension force based on the model proposed by Brackbill et al. (1992). The interface sharpening method and the surface tension force were validated on several test cases where viscosity was increased in order to achieve a damping of spurious currents. But up to now no transitions between small- and large scale gas phases have been considered.

The GENTOP-concept (Hänsch et al., 2012) enables to consider such transitions in a consistent way as coalescence and breakup processes. The potential of this concept was demonstrated in Hänsch et al. (2012) and Hänsch et al. (2014) for adiabatic flows without heat and mass transfer. In this paper the GENTOP concept is applied to simulate boiling effects in a vertical pipe where transitions from bubbly flow to churn turbulent and then annular flow are involved.

Boiling is a process in which heat transfer causes liquid evaporation. Flow boiling refers to a boiling process when the fluid is imposed by a forced flow. It can be classified as saturated boiling and subcooled boiling. In the saturated boiling, the bulk temperature of the fluid is as equal as its saturation temperature, in the subcooled boiling regime the bulk temperature of the fluid is less than its saturation temperature. Due to latent heat transport, boiling heat transfer plays a very important role in wide number of applications in many technological and industrial areas including nuclear reactor cooling systems, car cooling and refrigeration systems.

Flow boiling is considerably more complicated than pool boiling, owing to the simultaneous occurrence of hydrodynamics and boiling heat transfer processes. Flow boiling usually be characterized by the presence of thermodynamic non-equilibrium between the liquid and vapor phases. The capability to predict two-phase flow in the boiling region is of considerable interest in the safety analysis of systems which experience this phenomenon.

Thus, in order to fully understand and predict the boiling phenomenon, the high gas volume fractions must be taken into account. Realizing this need, the GENTOP concept was utilized and further developed for flows with heat and mass transfer in this

paper. It allows the modeling for bubbles smaller than the grid size and tracking the interface of large continuous bubbles (larger than the grid size). Thus, it is like a combination of Euler –Euler two fluid modeling and interface tracking techniques. It has been further advanced and validated for churn turbulent flow regimes (Montoya et al., 2014). The concept has not yet applied to the situation involving transitions from bubbly flows to churn turbulent and then annular flows. This paper presents a simulation of a generic boiling phenomenon in a vertical pipe with the help of the GENTOP concept in ANSYS-CFX, where important new models have been discussed and applied.

2. Morphology and gas-liquid flow regimes in pipes

Gas-liquid two-phase flows can appear in quite different topological or morphological configurations. These different structures are usually called flow regimes or flow patterns. Various physical transfer processes taking place across the phase-interface strongly depend on the flow regime.

The regimes encountered in vertical flows are illustrated in Fig. 2.1. They include bubble flow, where the liquid is continuous, and there is a dispersion of bubbles within the liquid; slug or plug flow where the bubbles have coalesced to make larger bubbles which approach the diameter of the tube; churn flow where heavily distorted large gas structures occur instead of well-shaped Taylor-bubbles; annular flow where the liquid flows on the wall of the tube as a film (with some liquid drops entrained in the core) and the gas flows in the center; and wispy annular flow where, as the liquid flow rate is increased, the concentration of drops in the gas core increases, leading to the formation of large lumps or streaks (wisps) of liquid.

3. CFD simulation of gas-liquid two phase flows

3.1. Continuity, momentum and energy equation

Multiphase CFD methods generally solve the conservation equations for mass, momentum and energy. One of the most frequently used frameworks for medium and large scale industrial problems is the two fluid Euler–Euler approach. This approach assumes that at least two fluids are continuously penetrating each other. The volume fraction of the fluids in each cell sums to unity. For each fluid, the full set of conservation equations is solved. Therefore, each fluid has a different velocity field. The certain morphology of one or the other phase is neglected. This enables the limitation of computational effort to be applied for industrial problems. The information lost by averaging has to be reappear in the closure relations describing the exchange between the phases. The mechanisms of the interaction of the fluids are the momentum transfer between the phase, the mass transfer modelled by phase change and the energy transfer. Mass conservation, momentum and energy conservation equations of the multi-fluid model are represented by the following equations:

$$\frac{\partial \alpha_k \rho_k U_k}{\partial t} + \nabla(\alpha_k \rho_k U_k) = \Gamma_K \tag{1}$$

$$\frac{\partial \alpha_k \rho_k U_k}{\partial t} + \nabla(\alpha_k \rho_k U_k U_k) = -\alpha_k \nabla p_k + \alpha_k \rho_k g + \nabla \alpha_k (\tau^v + \tau_k^t) + U_{k,i}\Gamma_k + M_{i,k} - \Delta\alpha_k \cdot \tau_i \tag{2}$$

$$\frac{\partial \alpha_k \rho_k H_k}{\partial t} + \nabla(\alpha_k \rho_k H_k v_k) = -\nabla \alpha_k (q^v + q_k^t) + \alpha_k \frac{D_k}{D_t}\rho_k + H_{ki}\Gamma_k + q''_{ki}/L_s + \Phi_k \tag{3}$$

where the subscript k denotes the phase and i stands for the value at the interface, denotes the length scale at the interface, ρ is the density, U is the velocity vector, t is the time, p is the pressure, g is the gravitational acceleration, α is the volume fraction, τ is the shear stress (τ^v is the average viscous shear stress, τ^t is the turbulent shear stress) τ_D is the interfacial shear stress, Γ_k is the mass generation, $M_{i,k}$ the generalized interfacial drag, q''_{ki} the interfacial heat flux and Φ_k the interfacial dissipation.

3.2. The generalized two phase flow (GENTOP) concept

The GEneralized TwO Phase flow (GENTOP) concept is based on a multi-field two-fluid approach. The flow is represented by a continuous liquid phase l, one or several poly-dispersed gas phases GasDi and a continuous gas phase GasC.

The dispersed gas GasD is modelled in the framework of the inhomogeneous Multiple Size Group (iMUSIG) -approach to deal with different bubble size groups and associated velocity fields (Frank et al., 2008). Within the poly-dispersed gas phases, transfers between different bubble size groups due to coalescence- and breakup as well as due to condensation and evaporation are taken into account by appropriate models.

The GENTOP concept has been developed as an extension of the inhomogeneous MUltiple SIze Group (iMUSIG) by adding a

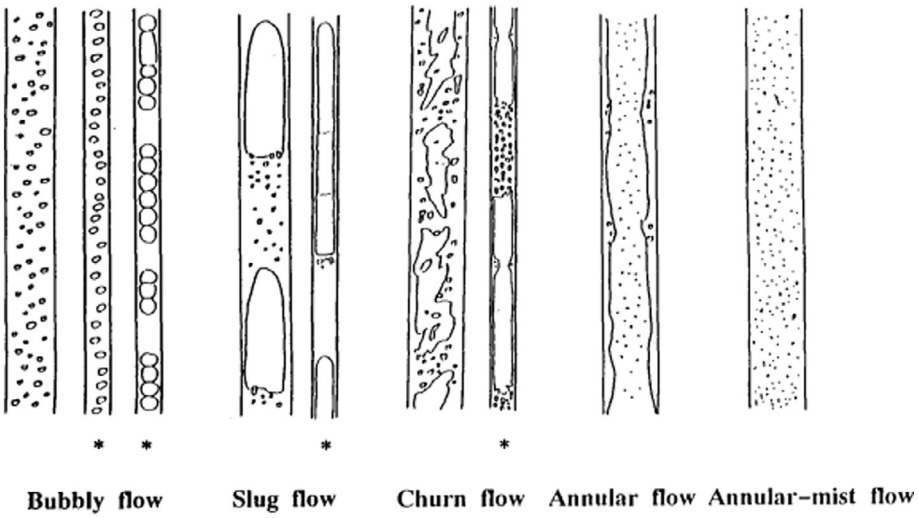

Fig. 2.1. Observed flow regimes (Ervin and Tryggvason, 1997).

potentially continuous gas phase GasC which is included within the MUSIG framework. (Fig. 3.1). This last velocity group represents all gas structures which are larger than an equivalent spherical bubble diameter, d_(dg,max). The interactions between GasC and the liquid phase are handled in a similar way like in the AIAD-concept (Höhne and Vallée, 2010). This includes the blending for bubbly flow, interface and droplet regions (see section 3.5) allowing to apply e.g. for a low volume fraction of GasC closures for bubbly flow. For this reason it is called potentially continuous phase Fig. 3.2.

In the actual paper the GENTOP concept is extended by mass and heat transfer (Fig. 3.1).

3.3. Turbulence modeling

In terms of turbulence treatment, the dispersed phase zero equation is used for the dispersed gaseous phases, while the SST k-ω approach is used for the liquid phase. One of the advantages of the k-ω model over the k-ε is the treatment when in low Reynolds numbers for a position close to the wall. The effect of bubbles on the liquid turbulence is considered by additional source terms (Rzehak and Krepper, 2013).

3.4. Inhomogeneous MUSIG model for poly-dispersed flows

The inhomogeneous multiple size group (iMUSIG) model, which bases on multi-fluid Euler–Euler approach, has been implemented into the ANSYS CFX code (Frank et al., 2008; Krepper et al., 2008). In this model the gaseous disperse phase is divided into a number M of MUSIG size fractions simulating bubble breakup&coalescence according to a population balance approach. To consider further the dependency of the momentum exchange between bubbles and liquid on the bubble size, several size fractions Mj are collected to N velocity groups, where each of the velocity groups is characterized by its own velocity field (see left part of Fig. 3.1).

Introducing ρ_G gas density and $\alpha_i = f_i \cdot \alpha_j$ as the gas volume fraction of the MUSIG group i (with $i = 1 \ldots \sum_{j=1}^{N} M_j$), which belongs to the velocity group j continuity equation for this group reads:

$$\frac{\partial}{\partial t}(\rho_g(\vec{r},t)\alpha_i(\vec{r},t)) + \frac{\partial}{\partial \vec{r}}(U_j(\vec{r},t)\rho_g(\vec{r},t)\alpha_i(\vec{r},t)) = \Gamma_i^{topo} \quad (4)$$

where $B_{B,i}$ and $B_{C,i}$ are the bubble birth rates due to breakup of larger bubbles into size group i and coalescence of smaller bubbles to MUSIG group i, respectively. Internally the conservation equations are formulated related on a discretisation regarding mass, i.e. bub-

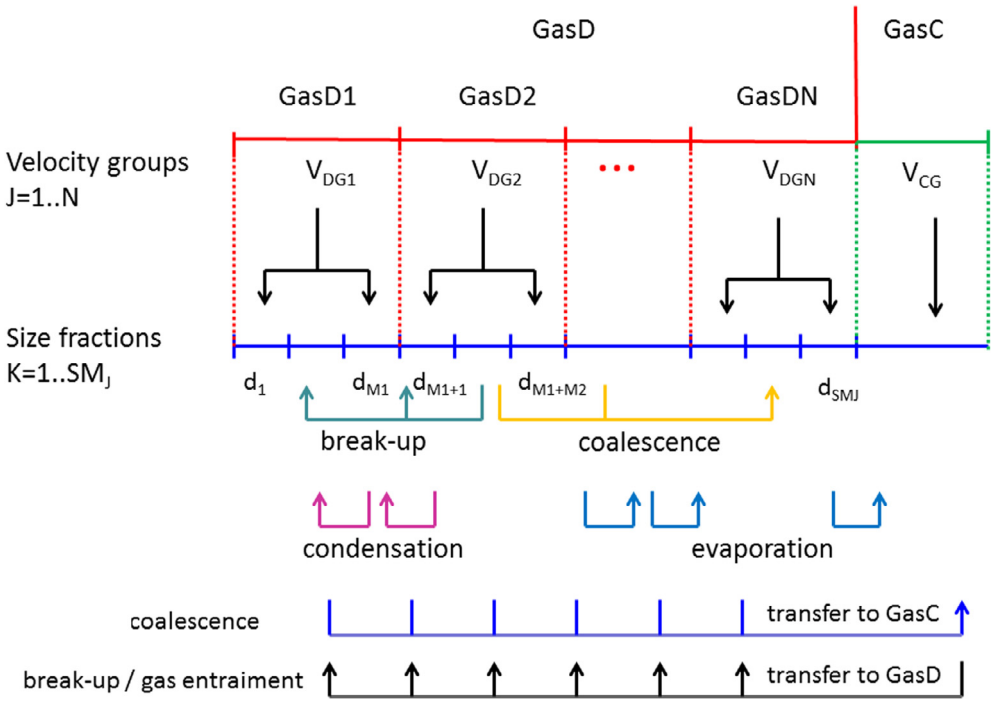

Fig. 3.1. Scheme of the extended GENTOP model including phase transfer.

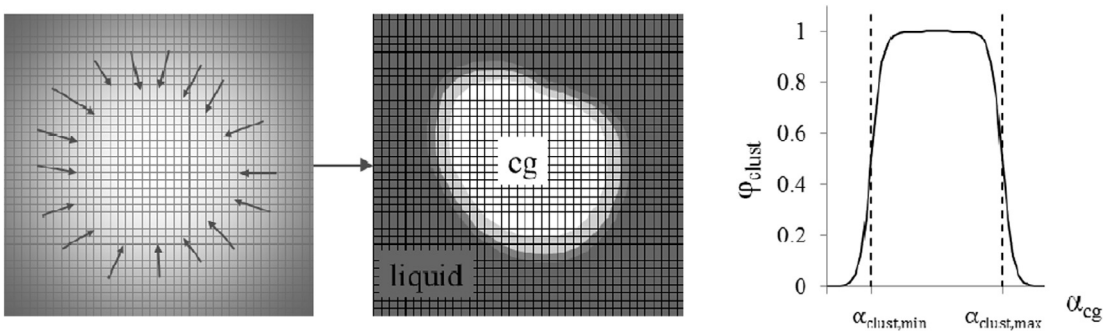

Fig. 3.2. Detail of a continuous gas liquid interface, and the blending function for a filtered interface (from Hänsch et al. (2012)).

ble size group boundaries are characterized by a fixed bubble mass. $D_{B,i}$ and $D_{C,i}$ are the bubble death rates due to breakup of bubbles from MUSIG group i into smaller bubbles and the coalescence of bubbles from size group i with other bubbles to even larger ones.

3.4.1. Modeling of momentum transfer between the dispersed phases and liquid

Due to the averaging of the conservation equations all information on the interface is lost, but has to be reintroduced by the use of closure relations. The closure laws objective is to account for the mass and momentum transfer between the different fields and phases while providing the functional form expected from the interfacial forces. The present models are limited by the need of local condition dependent coefficients, derived from the fact that the closure laws have been developed for ideal bubbly flow and are now being applied to churn-turbulent flow and slug conditions.

Rzehak et al. (2015) have tested and successfully validated a number of poly-dispersed closure laws for Euler-Euler calculations and set up a so called Baseline Model for multiphase poly-dispersed bubbly flows.

The total momentum exchange between dispersed gas and continuous liquid phase can be expressed as the superposition of several component forces (see Eq. (5)).

$$\mathbf{M}_k^i = \mathbf{M}_k^D + \mathbf{M}_k^{VM} + \mathbf{M}_k^{TD} + \mathbf{M}_k^L + \mathbf{M}_k^W \tag{5}$$

In the baseline model (Rzehak et al., 2015) the drag force $\mathbf{M}_k^D$ is calculated according to Ishii and Zuber (1979) (Table 3.1).

3.4.2. Breakup and coalescence model

The net mass source for size group *i* due to bubble coalescence and breakup can be expressed as the sum of bubble birth rates due to the breakup of larger bubbles from groups $j > i$ to group *i* and coalescence of smaller bubbles from size groups $j < i$, to group *i* as well as bubble death rates due to breakup of bubbles from size group *i* to smaller bubbles in groups $j < i$ and the coalescence of bubbles from size group *i* with bubbles from any other group to even larger ones which belong to groups $j > i$. That is,

$$\Gamma_i^{topo} = B_i^{break} - D_i^{break} + B_i^{coal} - D_i^{coal} \tag{6}$$

The birth and death rates in turn are commonly expressed in terms of the coalescence and breakup kernels. For the breakup and coalescence kernel functions *b* and *c* the commonly used breakup models according to Luo and Svendsen (1996) and the coalescence models of Prince and Blanch (1990) are applied in the present work, but were adjusted by factors F_B for breakup and F_C for coalescence. In this way the applicability of the general framework is demonstrated but of course further developments will be necessary to improve the physical models and overcome such tuning procedures. In our calculations, only breakup coefficient has been lowered to 0.01, due to high over prediction of breakup rates (Rzehak et al., 2015).

For details on modeling coalescence and breakup see Liao et al. (2015).

Table 3.1
Baseline model (Rzehak et al., 2015) for poly-dispersed flows used in GENTOP.

Model	Name
Drag coefficient ($C_{D,k}$)	Ishii and Zuber (1979)
Interfacial lift force	Tomiyama and Shimada (2002)
Turbulent dispersion force	Burns (2004)
Wall lubrication force	Hosokawa et al. (2002)

3.5. Handling of the potentially continuous phase GasC

3.5.1. Interface detection of the potentially continuous gas phase GasC

To resolve the interface of continuous gas structures, the interface has to be localized. This is based on an appropriate blending function Ψ_{surf} (Gauß and Porombka, 2015). It bases on the volume fraction and its gradient and is designed in a generalized form capable for later applications describing not only bubble regions but also droplet regions. It replaces the blending taken from the AIAD model (Höhne, 2014) which was combined with a volume fraction based interface function in the original GENTOP concept of Hänsch et al. (2012).

The interface blending function is defined as

$$\psi_{Surf} = \phi_{sf}(f_b - f_d) \tag{7}$$

which is equal to zero for at a interphase boundary. Additionally, it provides information about the morphology:

$$\psi_{Surf} = \begin{cases} 1 & \text{bubble region} \\ 0 & \\ & \text{interface} \\ -1 & \text{droplet region} \end{cases}$$

In the actual application only the bubble region and the interface region are of interest. The blending functions for the potentially continuous-phase bubble regime f_b and droplet regime f_d are given by:

$$f_b = \frac{1}{2}\left[1 + \cos\left(\pi \frac{\tilde{\alpha}^G - (\alpha_{b,crit} - \Delta_\alpha)}{2\Delta_\alpha}\right)\right] \tag{8}$$

$$f_d = \frac{1}{2}\left[1 + \cos\left(\pi \frac{\tilde{\alpha}^L - (\alpha_{d,crit} - \Delta_\alpha)}{2\Delta_\alpha}\right)\right] \tag{9}$$

The interface blending function is given by:

$$\phi_{sf} = \frac{1}{2}\left[1 + \cos\left(\pi \frac{\nabla\tilde{\alpha}^c - (\nabla\alpha_{crit} - \Delta_{\nabla\alpha})}{2\Delta_{\nabla\alpha}}\right)\right] \tag{10}$$

with $\alpha_{crit} = 0.3$ and $\Delta_{\nabla\alpha} = 0.05$.

3.5.2. Complete coalescence

During the calculation low fractions of dispersed gas in the region of mainly continuous gas might arise. To solve this unphysical situation a special coalescence method for complete gaseous mass transfer was established and is now included in the concept in order to replace the coalescence due to the averaged coalescence models when the critical void fraction is reached. The coalescence rate is turning all the remained dispersed gas, within a specific grid cell, into continuous gas. The complete coalescence is turned off inside the interface in order to allow coalescence and breakup at those positions. The mass transfer is defined by:

$$S_{GasD \to GasC} = (1 - |\Psi_{Surf}|)\,\rho_{dg}\alpha_{dg}/\tau \tag{11}$$

where $\tau_{dg \to cg} = \Delta t$ is a time constant that regulates how fast the mechanism occurs in consistency with the numerical scheme.

3.5.3. Clustering force GasC

The clustering force allows the transition from the dispersed towards the continuous gas phases using an aggregative effect within the volume fraction of the continuous gas. Modeling using an Eulerian approach will produce smearing of the volume fraction by numerical diffusion, thus this force produces interface stabilizing effects.

This force is an additional interfacial force acting exclusively between the continuous gas and the liquid phase and is included in the interfacial momentum transfer. This force acts proportion-

ally to the gradient of the volume fraction of the liquid as given in the following Eq. (12)

$$M_{cg}^{clust} = max(\phi_{chust,0}) c_{clust} \rho_l \nabla \alpha_l \quad (12)$$

As soon as the specific critical void fraction of continuous gas is reached, this force will create regions of continuous gas volume fraction by inducing aggregation on the continuous gas phase volume fraction until a complete formation of gas structures is reached. The force acts outside the interface region, agglomerating the gas, and blends out as soon as the critical gradient of volume fraction appears, completely disappearing as soon as a fully formed interface occurs ($\psi_{surf} = 0$). The clustering force disappears within the continuous structure. A constant value of $c_{clust} = 1$ is recommended for the GENTOP application.

3.5.4. Interfacial momentum transfer in GasC

The Algebraic Interfacial Area Density (AIAD) model, shown in Höhne and Mehlhoop (2014), allows detection of morphological form of two phase flow and is able to distinguish between bubbles, droplets and the interface through a corresponding switching via a blending function of each correlation from one object pair to another.

Based on Ψ_{surf} (blending function), formulations for interfacial area density and drag are defined as in Eqs. (13) and (14),

$$A_{GasC} = (1 - |\Psi_{surf}|)\, A_{fs} + a_{sign} |\Psi_{surf}|\, A_b + (1 - a_{sign}) |\Psi_{surf}| A_d \quad (13)$$

$$C_{D,GasC} = (1 - |\Psi_{surf}|)\, C_{D,fs} + a_{sign} |\Psi_{surf}|\, C_{D,b} + (1 - a_{sign}) |\Psi_{surf}| C_{D,d} \quad (14)$$

with $a_{sign} = \left\{ \begin{array}{l} 1 \ if \ sign(\Psi_{surf}) = 1 \\ 0 \ else \end{array} \right\}$.

Three different drag coefficients are applied:

1. $C_{D,bubb}$ (for bubbly regions): Ishii and Zuber Drag Formulation
2. $C_{D,drop}$ (for droplet regions): Drag coefficient is assumed constant and equal to 0.44
3. $C_{D,fs}$ (for interface region): The drag is ruled by viscous surface stresses and the formulation as proposed by Höhne and Mehlhoop (2014) is used.

$$C_{D,fs} = max\left[0.01, \frac{2[\alpha_l \tau_{w,l} + \alpha_{cg} \tau_{w,cg}]}{\rho_m u_{slip}^2}\right] \quad (15)$$

Similarly, the interfacial area density is applied as three different equations:

1. $A_{D,bubb}$ (based on particle model formulations)

$$A_{D,bubb} = \frac{6\alpha_{cg}}{d_{cg}} \quad (16)$$

2. $A_{D,drop}$ (based on particle model formulations)

$$A_{D,drop} = \frac{6\alpha_l}{d_l} \quad (17)$$

3. $A_{D,fs}$: For interface region, it depends on continuous gas and liquid both.

$$A_{D,fs} = \frac{(2|\Delta\alpha_l||\Delta\alpha_{cg}|)}{(|\Delta\alpha_l| + |\Delta\alpha_{cg}|)} \quad (18)$$

In our case, the minimum volume fraction of liquid (10^{-7}) is set inside the continuous phase, since no droplets are considered.

3.5.5. Turbulence damping liquid/GasC

Without any special treatment of the interface, the high velocity gradients at the interface, especially in the gaseous phase, generate levels of turbulence that are too high throughout the two-phase flow when using eddy viscosity models like the k-ε or the k-ω model. Therefore, a certain amount of damping of turbulence is necessary in the region of the interface, because the mesh is too coarse to resolve the velocity gradient in the gas phase at the interface.

For the two-fluid formulation, Egorov and Menter (2004) proposed a symmetric damping procedure. This procedure provides a solid wall-like damping of turbulence in both gas and liquid phases. More information can be found in Höhne and Mehlhoop (2014).

In the current version only damping from the liquid side is possible, since there is no turbulence model on the gas side in the code available.

3.5.6. Sub-grid wave turbulence Liquid/GasC

Small waves created by Kelvin-Helmholtz instabilities that are smaller than the grid size are neglected in traditional two phase flow CFD simulations, but the influence on the turbulence kinetic energy of the liquid side can be significantly large.

The consequence of the specific turbulent kinetic energy k_{SWT} is prescribed in a source term where the gradients of the local velocities and the liquid density are present and which is added to the total turbulent kinetic energy k (Wilcox, 1994). More information about the sub-grid wave turbulence is found in Höhne and Mehlhoop (2014).

3.5.7. Surface tension GasC

It is the force that exists at a interface and acts to minimize the surface area of the interface (Fig. 3.3). The fluid molecules which are on or near a liquid surface experience uneven molecular forces of attraction which causes the liquid surface to possess an elastic strength. This is the force of surface tension and is an inherent characteristic of the material interfaces.

If the interface is curved, it induces a force normal to the interface. The effect of this normal force is to smooth regions of high curvature; it tends to reduce the surface area of bubbles.

When the surface tension coefficient is not constant, the surface tension force has a tangential component which tends to move fluid along the interface towards regions of high surface tension

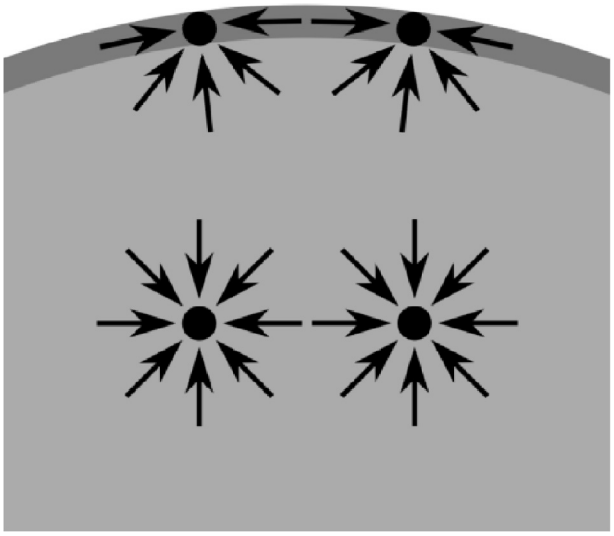

Fig. 3.3. Diagram of the forces on molecules of a liquid.

coefficient. This is generally caused by temperature gradients and is known as Marangoni effect.

The surface tension model which is used here is the Continuum Surface Force (CSF) model proposed by Brackbill et al. (1992). This model considers the surface tension force as a volume force concentrated at the interface, rather than a surface force. For a curved interface, the surface tension force can be written as:

$$M^{ST} = M_n^{ST} + M_t^{ST} \tag{19}$$

Where the normal component is given by:

$$M_n^{ST} = \sigma \kappa n \delta_s \tag{20}$$

n is the unit vector to the interface directed from the main to the secondary fluid.

In the CSF method, the δ_s distribution is approximated by:

$$\delta_s = |\nabla \alpha_i| \tag{21}$$

Using an elementary finite difference estimate of the normal yields:

$$n = -\frac{\nabla \alpha_i}{|\nabla \alpha_i|} \tag{22}$$

The curvature of the interface is calculated in terms of divergence of the normal vector. Thus, the normal component of the surface tension force is given by:

$$M_n^{ST} = -\sigma * \nabla \cdot \left(\frac{\nabla \alpha_i}{|\nabla \alpha_i|}\right) * \nabla \alpha_i \tag{23}$$

And the tangential component of the surface tension force is:

$$M_t^{ST} = \frac{d\sigma}{dt} T = \nabla \sigma * |\nabla \alpha_i| \tag{24}$$

We have assumed a constant value of surface tension coefficient, thus the tangential component of surface tension force is zero.

The actual implementation of the surface tension force in the CFD-code CFX is unfortunately limited only to a two phase flow application. Therefore for the actual three phase flow the force has to be implemented again.

3.6. Phase change model for GasD and GasC

3.6.1. Interphase heat transfer models

For the simulation of boiling, the thermal phase change model has been used for the disperse gas phase (GasD) and liquid pair and the continuous gas phase (GasC) and liquid pair.

Due to thermal non-equilibrium, heat transfer occurs across the phase interface. It is described in terms of an overall heat transfer coefficient h_{LG}, which is the amount of heat energy crossing a unit area per unit time per unit temperature difference between the phases. Rate of heat transfer Q_{LG} per unit time across a phase boundary of interfacial area per unit volume A_D, from liquid to gas, is:

$$Q_{LG} = h_{LG} A_D (T_G - T_L) \tag{25}$$

Or, this can be rewritten as:

$$Q_{LG} = c_{LG}^{(h)} (T_G - T_L) \tag{26}$$

$c_{LG}^{(h)} = h_{LG} A_D$ for the particle model that we have used in the case.

Hence, the interfacial area per unit volume and the heat transfer coefficient h_{LG} needs to be known.

We know that $h = \frac{\lambda Nu}{d}$

In the particle model, λ is taken to be the thermal conductivity of the continuous phase and the length scale d is the mean diameter of the dispersed phase, that is:

$$h_{LG} = \frac{\lambda_L Nu_{LG}}{d_G} \tag{27}$$

In our case of heat transfer between liquid and gas, the use of overall heat transfer coefficient is not sufficient to model the interphase heat transfer process. This model considers separate heat transfer process on each side of the phase interface. This is achieved by using two heat transfer coefficients defined on each side of the phase interface.

The sensible heat flux to liquid from the interface is given as:

$$q_L = h_L (T_s - T_L) \tag{28}$$

Similarly, the sensible heat flux to gas from the interface:

$$q_G = h_G (T_s - T_G) \tag{29}$$

The fluid specific Nusselt number is given by:

$$Nu_L = \frac{h_L d_{LG}}{\lambda_L} \tag{30}$$

The interphase mass transfer is determined from the total heat balance:

Total heat flux to phase L from the interface:

$$Q_L = q_L + \dot{m}_{LG} H_{LS} \tag{31}$$

Total heat flux to phase G from the interface:

$$Q_G = q_G + \dot{m}_{LG} H_{LS} \tag{32}$$

H_{LS} and H_{GS} represent interfacial values of enthalpy carried into and out of the phases du to phase change. The total heat balance $Q_G + Q_L = 0$ now determines the interphase mass flux:

$$\dot{m}_{LG} = (Q_L + Q_G)/(H_{GS} - H_{LS}) \tag{33}$$

For spherical bubbles the Ranz Marshall or Hughmark correlation can be applied to calculate the Nusselt number. In the present simulation the Ranz and Marshall (1952) correlation was used for the disperse gas phase (GasD) and liquid pair. The correlation is given as:

$$Nu = 2 + 0.6 Re_{slip}^{0.5} Pr^{0.3} \tag{34}$$

with Re_{slip} as the slip velocity Reynolds number:

$$Re_{slip} = \frac{U_{slip} \cdot d}{\nu} \tag{35}$$

With d equal to the mean particle diameter.and the Prandtl number Pr:

$$Pr = \frac{\eta \cdot c_p}{\lambda} \tag{36}$$

It is based on boundary layer theory for steady flow past a spherical particle and thus is not valid for the GasC – liquid transfer.

For the potentially continuous gas phase (GasC) and liquid pair the Hughes Duffey correlation was used (Hughes and Duffey (1991)):

$$Nu = 1.13 + Re_{turb} Pr^{0.5} \tag{37}$$

where Pr is Prandtl number and Re_{turb} turbulent Reynolds number of liquid.

Here, the turbulent Reynolds number is calculated from local parameters as:

$$Re_{turb} = \frac{U_{turb} \cdot L_{turb}}{\nu} \tag{38}$$

where ν_L is liquid viscosity, L_{Turb} is length scale and U_{Turb} velocity scale, which are calculated from liquid turbulence kinetic energy k_L and turbulence dissipation ε_L:

$$U_{turb} = C_\mu^{1/4} k_L^{1/2}, C_\mu = 0.09 \tag{39}$$

$$L_{turb} = C_\mu \frac{k_L^{3/2}}{\varepsilon_L} \tag{40}$$

3.6.2. Condensation and evaporation including boiling at the wall GasD

When condensation or evaporation occur, the volume fraction in size group i changes for two reasons: (i) mass is transferred directly between the bubbles and the liquid and (ii) since due to this direct mass transfer the bubbles are shrinking or growing they may subsequently belong to a different size group.

Written as a source term for size group i the direct mass transfer to the liquid is given by

$$\tilde{\Gamma}_i = -\frac{A_{I,i}}{H_{LG}} h_{L,i}(T_L - T_{sat}), \tag{41}$$

where similar to previous work (Krepper and Rzehak, 2011) the assumption has been made that the gas is at saturation temperature. The total source terms for size class i including also the ensuring change of bubble size, i.e. Γ_i^{phase} in Eq. (33), has been derived recently by Lucas et al. (2011) as

$$\Gamma_i^{phase} = \begin{cases} \frac{m_i}{m_i - m_{i-1}} \tilde{\Gamma}_i - \frac{m_i}{m_{i+1} - m_i} \tilde{\Gamma}_{i+1} \; for \; \tilde{\Gamma}_i < 0, \text{i.e. condensation} \\ \frac{m_i}{m_i - m_{i-1}} \tilde{\Gamma}_{i-1} - \frac{m_i}{m_{i+1} - m_i} \tilde{\Gamma}_i \; for \; \tilde{\Gamma}_i > 0, \text{i.e. evaporation} \end{cases}, \tag{42}$$

where $m_i = \rho \, \pi \, d^3/6$ is the mass of each bubble in size group i. Basing the calculation on bubble mass rather than size for compressible flows has the advantage that since mass is conserved no extra terms arise in the equations. Conversion to the corresponding bubble size which depends on the local density can be done straight forwardly as needed. For incompressible flows, no differences between mass- and size-based groups arise.

In principle $\tilde{\Gamma}_i$ should be evaluated with the group size d_i, but for practical reasons an approximation is used where a mass transfer term $\tilde{\Gamma}_j$ is calculated only for each velocity group j using the Sauter mean diameter and the area based fraction thereof is used for $\tilde{\Gamma}_i$, i.e.

$$\tilde{\Gamma}_i = \frac{A_{I,i}}{A_{I,j}} \tilde{\Gamma}_j. \tag{43}$$

In this way, the size dependency of the factor $A_{I,i}$ in Eq. (35) is treated exactly, but that of the factor $h_{I,i}$ is not. The liquid side heat transfer coefficient, finally is calculated according to Ranz and Marshall (1952) as

$$h_L = \frac{k_L}{d_B} Nu = \frac{k_L}{d_B} \left(2 + 0.6 \mathrm{Re}^{1/2} \mathrm{Pr}^{1/3}\right). \tag{44}$$

In addition to the source terms for the continuity equations for the bubble size groups there is also a mass source for the liquid phase continuity equation which is given by

$$\Gamma_L = -\sum_i \tilde{\Gamma}_i. \tag{45}$$

Moreover, corresponding secondary sources appear in the momentum and energy equations.

A validation of the above procedure against experimental data has been given by Krepper et al. (2013).

To include the generation of vapor bubbles at the wall, an additional source term, S_{rpi}, is included according to Eq. (27). This source term applies only to the equation corresponding to the size group whose diameter is the closest to the bubble detachment diameter d_W. It is given by the evaporation mass flux computed in the wall heat partitioning distributed evenly throughout the grid cells adjacent to the heated wall, i.e.

$$S_{rpi} = \dot{m}_W \frac{S}{V}, \tag{46}$$

where $\dot{m}_W$ is given and S and V are wall surface area and volume of the corresponding grid cell, respectively.

3.6.3. Wall boiling model GasD

The wall boiling model is only activated for the disperse gas phase (GasD) and liquid pair. Initially, water is below its saturation temperature. Water becomes supersaturated locally, leading to the formation of bubbles. The bubbles will start departing and before the formation of next bubble, some of heat will go in superheating the water. This process is known as *quenching*. In regions of the wall not affected by bubble growth, wall heat transfer to the water is described by single phase convective heat transfer.

In the actual paper the wall boiling heat flux partitioning model developed at RPI and implemented in CFX (ANSYS CFX, 2015) with its basic submodels and parameters is applied.

Hence, in total, there is a 3 way partition of the wall heat flux:

$$Q_w = Q_c + Q_q + Q_e \tag{47}$$

Thus, the area of a wall is partitioned into 2 parts:

1. Fraction A_2, influenced by the vapor bubbles
2. Fraction A_1, the rest of the wall $(1 - A_2)$

Convective heat flux Q_c is given as:

$$Q_c = A_1 h_c (T_w - T_1) \tag{48}$$

Similarly, heat flux consumed for the evaporation of initially sub-cooled water:

$$Q_e = \dot{m}(h_{g,sat} - h_1) \tag{49}$$

And the heat flux consumed for quenching:

$$Q_q = A_2 h_q (T_w - T_1) \tag{50}$$

The area fraction values A_1 and A_2 are related to the nucleation site density per unit wall area n and the influence area of a single bubble forming at the wall nucleation site. The latter is modelled with the bubble departure diameter value d_w which serves as a length scale of the wall boiling mechanism. The non-dimensional area fraction of the bubble fraction is taken as:

$$A_2 = min(\pi d_w^2 . n, 1) \tag{51}$$

A detailed discussion of the aspects of wall boiling can be found in Krepper et al. (2013) and Rzehak et al. (2014).

4. Demonstration case of a side wall heated tube

To illustrate the previous described concept a demonstration example of a vertical side wall heated tube is given. The tube has a length of 0.5 m and a diameter of 0.025 m. Water is considered at a pressure of 5 MPa. At this pressure the saturation temperature amounts to 537 K. The initial temperature was set to a subcooling of 3 K. The temperature of the heated wall is set to a superheating of 10 K. The inlet velocity is 0.2 m/s.

4.1. Geometry, mesh and general setup

The pipe is presented by a fully 3D geometry shown in Fig. 4.1 along with the name of the different zones (i.e., inlet, hot wall and outlet). The resulting mesh is made of approximately 130,000 hexahedral cells. A grid resolution study was conducted to ensure that

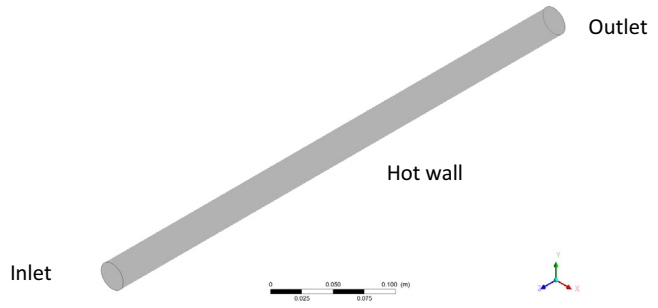

Fig. 4.1. Pipe geometry.

convergence with respect to the spatial resolution has been achieved. The grid spacing is on average 2 mm. The solver y + ranges from 25 to 75 at the wall region. A multiphase simulation was set up. Gas was described in the inhomogeneous poly-dispersed multiple size group (iMUSIG) framework by the dispersed gaseous phases GasD1 and GasD2 and the continuous gas phase GasC.

A total of four velocity fields, three gas and one for the continuous liquid were solved. Gas was assumed at saturation temperature. Properties of dry steam at saturation temperature have been taken from the steam tables. At the hot wall a wall boiling model generating GasD was applied. GasC then arise either by coalescence of GasD or by evaporation in the bulk. The following table shows the numerical scheme used in the case (Table 4.1):

The simulations were run on the HZDR Linux-Cluster hydra. It consists of two heads and 72 compute nodes. Each node has 2 Intel CPUs (Xeon 8-Core or 16-Core). In general hydra consists of more than 1500 CPU-cores and 8,5 TB of main memory. The network is a 1GbE Ethernet and additionally an InfiniBand fabric with a bandwidth of 40 Gbit/s, which qualifies hydra for sequential, coarse granularity parallel and massively parallel jobs. The operating system is Ubuntu Linux. The theoretical general peak performance (single precision) amounts to 70,5 TFlop/s.

ANSYS CFX (2015) is an element-based finite-volume method with second-order discretisation schemes in space and time. It uses a coupled algebraic multigrid algorithm to solve the linear systems arising from discretisation. The discretisation schemes and the multigrid solver are scalably parallelized.

The calculation of 7 s real time took 4 days, 11 h on 32 processors.

4.2. Overview of the settings and models used in the GENTOP framework

For the specified fluid water/steam at a pressure of 5 MPa the critical bubble size, were the lift coefficient changes its sign, is found for $d_B = 4$ mm. For GasD (dispersed gas) the iMUSIG model with 4 size fractions for GasD1 and 5 size fractions for GasD2 was applied. An equidistant bubble size distribution with a size difference of 1 mm was assumed. In this way the lift coefficient for GasD1 is clear different from the lift coefficient of GasD2. GasC was considered as last size fraction of the iMUSIG framework, to include it in the coalescence and fragmentation process. All gas structures equal or larger than 10 mm sphere equivalent diameter are assigned to GasC. The coalescence and breakup models according to Luo and Svendsen (1996) and Prince and Blanch (1990) with coefficients of $F_B = 0.01$ and $F_C = 4$ were applied.

Momentum exchange between GasD and liquid was simulated considering all usually applied exchange terms for drag and non-drag forces were used. Concerning the drag between GasC and Liquid the formulation of AIAD was applied (Hänsch et al., 2014).

Table 4.1
Solver setup.

Advection scheme	Option	High resolution
Transient scheme	Option	Second Order Backward Euler
	Δt	0.005 s
Convergence control	Timescale control	Coefficient loops
	Min./max. coeff. loops	4/50
Convergence criteria	Residual type	RMS
	Residual target	1e−04

The liquid phase was simulated as turbulent using the shear stress transport model. The influence of bubbles of GasD on the liquid turbulence was considered.

The implementation of the GENTOP framework followed generally the models described in section 3. The exchange models were implemented using subdomains. Surface tension for the pair GasC and Liquid was implemented (3.5.7). Effects of numerical diffusion were compensated by an additional force, the Clustering force acting between GasC and Liquid to keep the interface between GasC and Liquid stable (3.5.3). The disappearance of unphysical fractions of dispersed gas in zones of prevailing GasC was enforced by complete coalescence (3.5.2).

Concerning the turbulence of the liquid at the presence of an interface to GasC experiences with the AIAD model were used. Turbulence damping at the interface was considered (3.5.5) and waves smaller as the grid resolution were treated as in the AIAD model (3.5.6).

5. Results and discussion

Fig. 4.2 shows the time course of the volume the averaged parameters in the whole flow domain. During the first 0.3 s only dispersed gas is generated by boiling (see Fig. 4.2b). After this time also continuous gas arises, mainly by coalescence of dispersed gas. After about 1 s the whole domain is heated up.

In Fig. 4.3 the cross sectional averaged values of liquid temperature (a) and gas volume fractions (b to c) dependent on the height z are shown. Especially Fig. 4.3 d for time averaged values (3..13 s) shows that in the lower part of the first 0.1 m of the tube only dispersed gas is generated. Fig. 4.4 presents gas volume fractions for dispersed gas (GasD), continuous gas (GASC) and the sum of both (GasTot) after a heating time of 2.0 s. During this time a steady state oscillating period is reached.

At the beginning of the heating up process mainly small bubbles occur near the wall. The wall boiling model releases bubbles having a diameter of about 1 mm. By the agglomerative effect of the cluster-force and using the principles of the GENTOP-concept it is possible to create continuous gas structures out of a dispersed gas phase as demonstrated in Fig. 4.4. After the wall boiling of small bubble sizes the domain with the smallest bubble size group the dispersed gas phase is characterized by an increase of mean bubble diameter due to the coalescence processes in the MUSIG-framework. When the mass transfer to the continuous gas begins and the volume fraction of GasC exceeds the threshold value $\alpha_{cg} > \alpha_{clust,min}$, here set to 0.5, the cluster-force agglomerates the continuous volume fraction until the complete coalescence replaces the dispersed gas fractions and large gas structures are resolved. They further coalesce to larger gas structures forming distorted cap-bubbles and larger slugs represented in the picture (Fig. 4.4). In grid cells where the continuous gas volume fraction stays below the threshold value $\alpha_{cg} < \alpha_{clust,min}$ the gas is treated as a dispersed phase following the particle model formulations.

Close observation of the GasD and GasC/Liquid interface show that the flow regimes discussed in section 2 and shown in Fig. 2.1 except the annular mist flow regime can be found in the simulation.

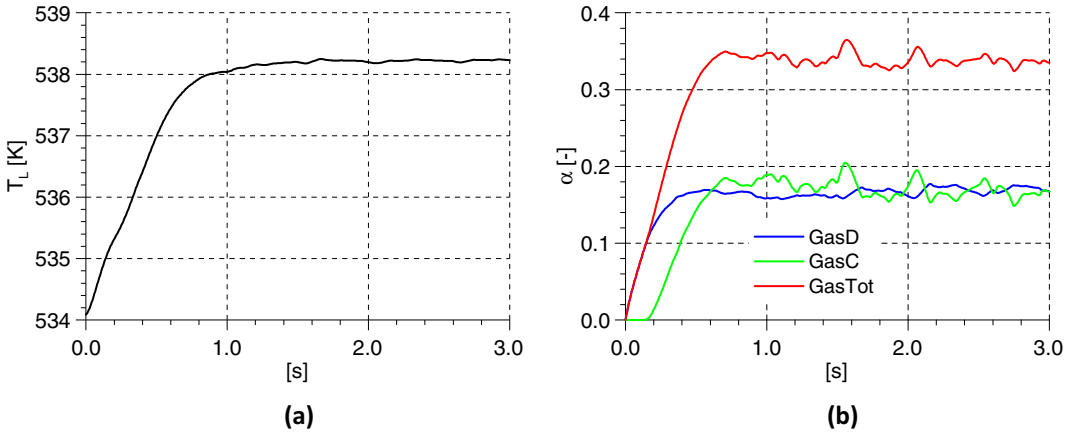

Fig. 4.2. Time course of the averaged liquid temperature (left) and the volume fractions for dispersed and continuous gas (right).

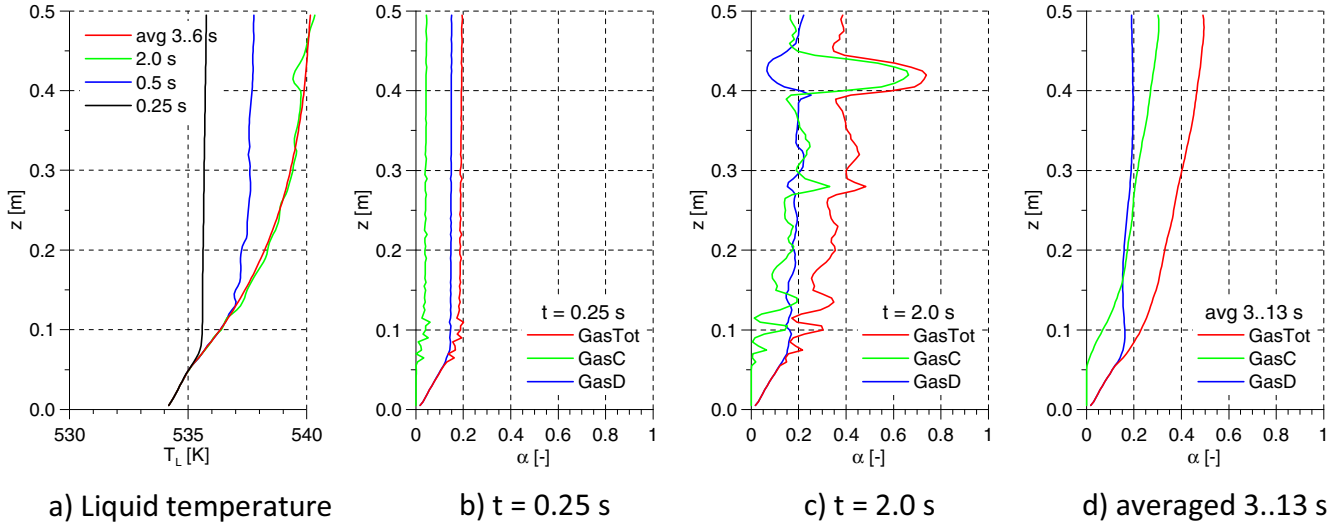

Fig. 4.3. Cross sectional averaged profiles for the liquid temperature (a) and the gas volume fractions for different times (b–c). (d) Presents time averaged values.

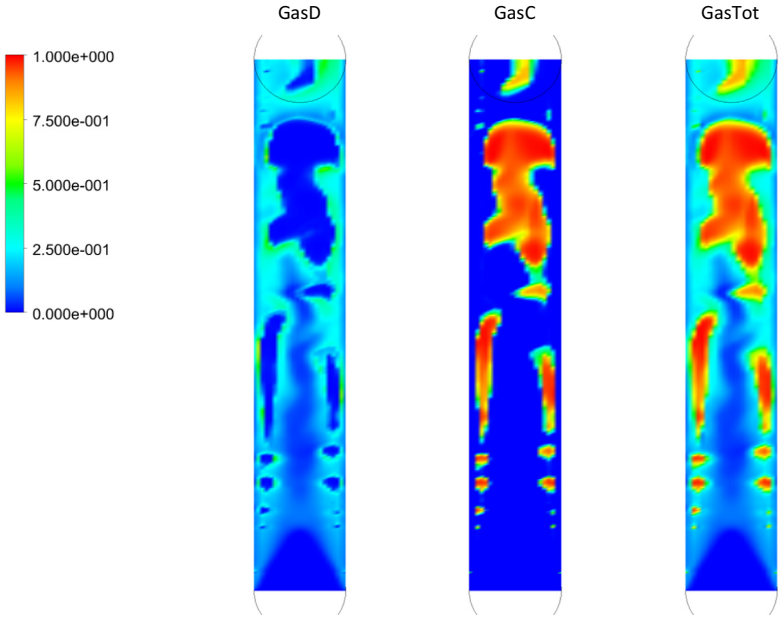

Fig. 4.4. Distribution of the gas volume fraction at 2.0 s (stretched height).

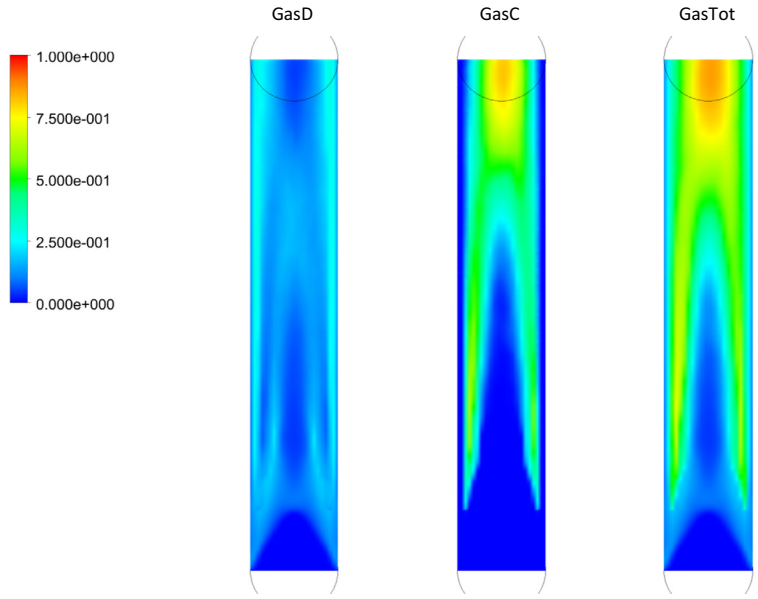

Fig. 4.5. Distribution of the gas volume fraction time averaged (stretched height).

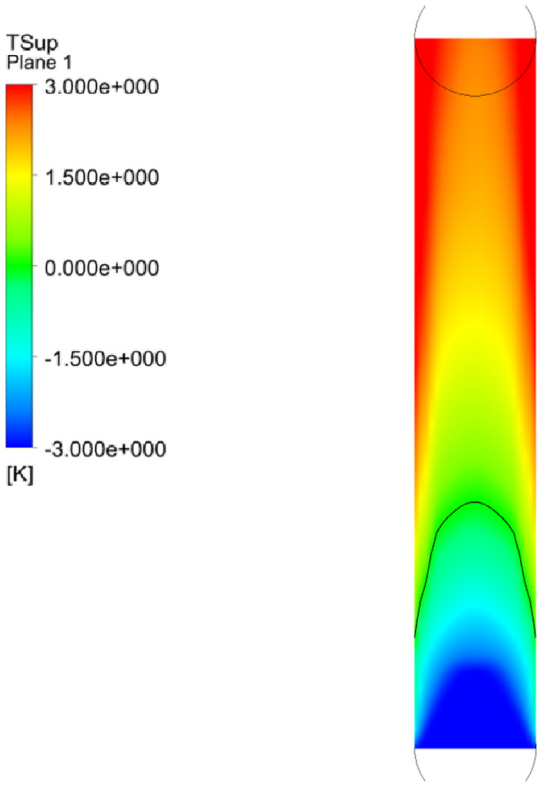

Fig. 4.6. Time averaged superheating liquid temperature.

The bubble flow regime occurs at relatively low gas flow rates, for which the gas phase appears in the form of small bubbles in the lower part of the pipe. Later bubbly–slug flow is characterized by the presence of relatively large cap-shaped bubbles, which occupy nearly the entire pipe cross-section and flow alongside smaller, deformable bubbles.

Fig. 4.5 shows time averaged gas volume fractions. Here the tendency to annular flow can be seen clearly. The churn turbulent flow appears to be highly chaotic and frothy and may seem to move upwards at some instants and downwards at other instants. Also in the annular flow regime at the end of the pipe, one may notice the existence of a gas core and a relatively uniform annular liquid film on the pipe wall as well as liquid slugs. The annular film mostly moves upwards but occasionally may seem to pause. This pause occurs when a liquid slug fills the local cross-section of the pipe, thus blocking the flow of gas in the core. Shortly afterwards, however, the liquid slug gets penetrated by gas and the upward annular-type flow is resumed.

Fig. 4.6 presents time averaged (3..13 s) liquid superheating temperature (Tsup = TLiq − Tsat). The black line marks the boundary for Tsup = 0. Above this line the fluid is superheated.

Fig. 4.7 represents essential GENTOP parameters at 2 s. The interface detection (3.5.1) marks the identified interface. The cluster force is acting stabilizing the interface between GasC and Liquid. From the other side the surface tension force is acting in contradiction to the cluster force.

6. Summary and outlook

The GENTOP concept, which allows dealing with configurations involving dispersed and continuous interfacial structures, was coupled with a wall boiling model and extended to consider heat and mass transfer between gas and liquid in the bulk. New model aspects of GENTOP were implemented and tested. Starting with a sub-cooled liquid in a hot pipe, bubbles (boiling) start to appear as soon as the liquid reaches its saturation temperature.

Since, the temperature of pipe wall is above the saturation temperature of the liquid, a series of flow regimes appear starting from bubbly flow, churn turbulent flow to annular flow. The simulation of the transitions between different flow regimes during boiling in a pipe is now feasible. Next the demonstration case using the GENTOP-concept will follow experiments for a qualitative comparison of simulation results. The GENTOP sub-models and the Wall Boiling Model need a constant improvement and separate, intensive validation effort.

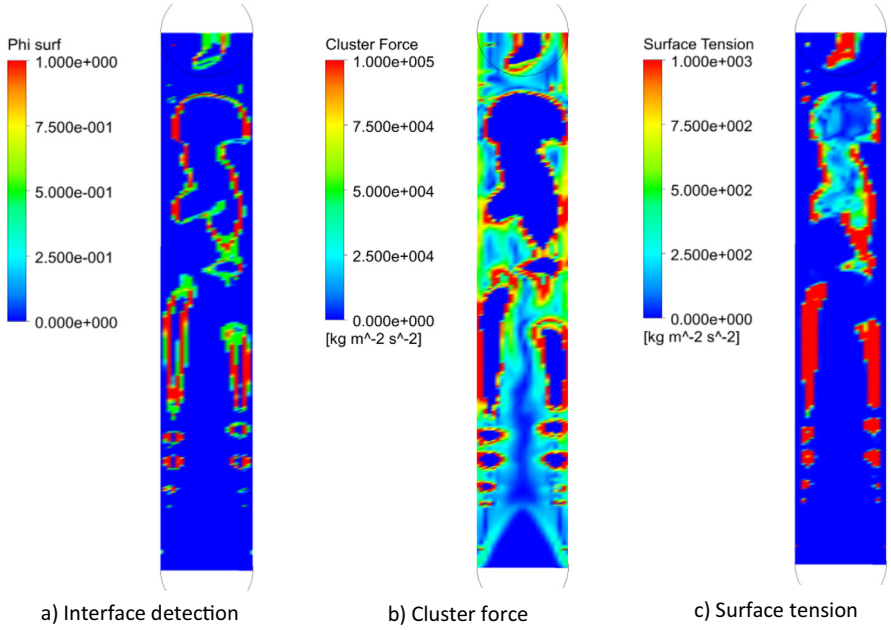

Fig. 4.7. Essential parameters of the GENTOP model framework at t = 2 s.

References

ANSYS CFX, 2015. User Manual. Ansys Inc.

Bartosiewicz, Y., Seynhaeve, J.-M., Vallée, C., Höhne, T., Laviéville, J.-M., 2010. Modelling free surface flows relevant to a PTS scenario: comparison between experimental data and three RANS based CFD-codes. Comments on the CFD-experiment integration and best practice guideline. Nucl. Eng. Des. 240, 2375–2381.

Bestion, D., 2010. Applicability of two-phase CFD to nuclear reactor thermohydraulics and elaboration of best practice guidelines. In: Proc. CFD4NRS-3, September 14–16, Washington DC, USA.

Brackbill, J., Kothe, D.B., Zemach, C., 1992. A continuum method for modeling surface tension. J. Comput. Phys. 100 (2), 335–354.

Burns, A.D., et al, 2004. The Favre averaged drag model for turbulent dispersion in Eulerian multi-phase flows. In: 5th International Conference on Multiphase Flow, ICMF.

Coste, P., Laviéville, J., Pouvreau, J, Baudry, C., Guingo, M., Douce, A., 2010. Validation of the large interface method of NEPTUNE_CFD 1.0.8 for pressurized thermal schock (PTS) applications. In: Proc. CFD4NRS-3, September 14–16, Washington DC, USA.

Egorov, Y., Menter, F., 2004. Experimental implementation of the RPI boiling model in CFX-5.6. Technical Report ANSYS/TR-04-10.

Ervin, E., Tryggvason, G., 1997. The rise of bubbles in a vertical shear flow. J. Fluids Eng. 119 (2), 443–449.

Frank, T., Zwart, P.J., Krepper, E., Prasser, H.-M., Lucas, D., 2008. Validation of CFD models for mono- and polydisperse air-water two-phase flows in pipes. Nucl. Eng. Des. 238, 647–659.

Gauß, F., Porombka, P., 2015. Internal HZDR Communication.

Hänsch, S. et al., 2012. A multi-field two-fluid concept for transitions between different scales of interfacial structures. Int. J. Multiphase Flow 47, 171–182.

Hänsch, S., Lucas, D., Höhne, T., Krepper, E., 2014. Application of a new concept for multi-scale interfacial structures to the dam-break case with an obstacle. Nucl. Eng. Des. 279, 171–181.

Höhne, T., Mehlhoop, J.-P., 2014. Validation of closure models for interfacial drag and turbulence in numerical simulations of horizontal stratified gas–liquid flows. Int. J. Multiphase Flow 62, 1–16.

Höhne, T., Vallée, C., 2010. Experiments and numerical simulations of horizontal two-phase flow regimes using an interfacial area density model. J. Comput. Multiphase Flows 2 (3), 131–143.

Höhne, T., Deendarlianto, Lucas, D., 2011. Numerical simulations of counter-current two-phase flow experiments in a PWR hot leg model using an area density model. Int. J. Heat Fluid Flow 32 (5), 1047–1056.

Hosokawa, S., Tomiyama, A., Misaki, S., Hamada, T., 2002. Lateral Migration of Single Bubbles Due to the Presence of Wall. In: Proc. ASME Joint U.S.-European Fluids Engineering Division Conference (FEDSM2002), Montreal, Quebec, Canada (Vol. ASME Conf. Proc. 2002 Vol. 1: Fora, Parts A and B, 855).

Hughes, E., Duffey, R., 1991. Direct contact condensation and momentum transfer in turbulent separated flows. Int. J. Multiphase Flow 17, 599–619.

Ishii, M., Zuber, N., 1979. Drag coefficient and relative velocity in bubbly, droplet or particle flows. AIChE J. 25, 843–855.

Krepper, E. et al., 2008. The inhomogeneous MUSIG model for the simulation of poly-dispersed flows. Nucl. Eng. Des. 238 (7), 1690–1702.

Krepper, E., Rzehak, R., 2011. CFD for subcooled flow boiling: Simulation of DEBORA experiments. Nucl. Eng. Des. 241, 3851–3866.

Krepper, E., Rzehak, R., Lifante, C., Frank, T., 2013. CFD for subcooled flow boiling: coupling wall boiling and population balance models. Nucl. Eng. Des. 255, 330–346.

Liao, Y., Rzehak, R., Lucas, D., Krepper, E., 2015. Baseline closure model for dispersed bubbly flow: bubble coalescence and breakup. Chem. Eng. Sci. 122, 336–349.

Lucas, D.M., Frank, T., Lifante, C., Zwart, P., Burns, A., 2011. Extension of the inhomogeneous MUSIG model for bubble condensation. Nucl. Eng. Des. 241, 4359–4367.

Luo, H., Svendsen, H.F., 1996. Theoretical model for drop and bubble breakup in turbulent dispersions. AIChE J. 42 (5), 1225–1233.

Montoya, G., et al. 2014. Analysis and applications of a generalized multi-field two-fluid approach for treatment of multi-scale interfacial structures in high void fraction regimes. In: Proc. Int. Congress on Adv. on Nucl. Power Plants. ICAPP2014-14230, USA.

Olsson, E., Kreiss, G., 2005. A conservative level set method for two phase flow. J. Comput. Phys. 210, 225–246.

Porombka, P., Höhne, T., 2015. Drag and turbulence modelling for free surface flows within the two-fluid Euler-Euler framework. Chem. Eng. Sci. 134, 348–359.

Prince, M.J., Blanch, H.W., 1990. Bubble coalescence and break-up in air-sparged bubble columns. AIChE J. 36 (10), 1485–1499.

Ranz, W., Marshall, W., 1952. Evaporation from drops. Chem. Eng. Prog 48 (3), 141–146.

Rzehak, R., Krepper, E., 2013. CFD modeling of bubble-induced turbulence. Int. J. Multiphase Flow 55, 138–155.

Rzehak, R., Ziegenhein, T., Liao, Y., Kriebitzsch, S., Krepper, E., Lucas, D., 2015. Baseline model for simulation of bubbly flows. Chem. Eng. Technol. 38, 1972.

Štrubelj, L., Tiselj, I., Mavko, B., 2009. Simulations of free surface flows with implementation of surface tension and interface sharpening in the two-fluid model. Int. J. Heat Fluid Flow 30, 741–750.

Tomiyama, A., Shimada, N., 2002. (N + 2)-field modeling for bubbly flow simulation. Comp. Fluid Dyn. J. 9 (4), 418–426.

Tomiyama, A., Sakoda, K., Hayashi, K., Sou, A., Shimada, N., Hosokawa, S., 2006. Modeling and hybrid simulation of bubbly flow. Multiphase Sci. Tech. 18 (1), 73–110.

Vallée, C., Höhne, T., Prasser, H.-M., Sühnel, T., 2008. Experimental investigation and CFD simulation of horizontal stratified two-phase flow phenomena. Nucl. Eng. Des. 238, 637–646.

Wilcox, D.C., 1994. Turbulence Modelling for CFD. DCW Industries Inc, La Cañada, California.

Zwart, P. J., Burns, A. D., Galpin, P.F., 2007. Coupled Algebraic Multigrid for Free Surface Flow Simulations. In: Proc. 26th Int. Conf. on offshore mechanics and arctic engineering, OMAE2007-29080.